MODELING THE STRUCTURE FUNCTIONS IN LINEARLY FORCED ISOTROPIC TURBULENCE

Evangelos Akylas
Department of Civil Engineering and Geomatics
Cyprus University of Technology, Limassol, Cyprus
evangelos.akylas@cut.ac.cy

Elias Gravanis
Department of Civil Engineering and Geomatics
Cyprus University of Technology, Limassol, Cyprus
elias.gravanis@cut.ac.cy

Marios Fyrillas
Department of Mechanical Engineering,
Frederick University, Nicosia, Cyprus
m.fyrillas@gmail.com

Damian I. Rouson
Sandia National Laboratories,
Livermore, CA 94550, United States
rouson@sandia.gov

Stavros C. Kassinos
Department of Mechanical and Manufacturing Engineering,
Computational Sciences Laboratory, UCY-COMPSCI
University of Cyprus, Nicosia, Cyprus
kassinos@ucy.ac.cy

ABSTRACT

The physics of the linear forcing of isotropic turbulence, allows for some useful estimates of the characteristic length scales of the turbulence produced during the statistically stationary phase. With such estimates we could practically define uniquely the stationary statistics by means of the box-size of the simulation, the linear forcing parameter and the viscosity of each case. We use such estimations in the Karman-Howarth equation and we solve it in terms of the second and third order structure functions using a generalized Oberlack-Peters closure scheme. The resulting forms and the respective spectra are in very good agreement with experimental and DNS data.

INTRODUCTION

Numerical simulations of isotropic turbulence play a key role in studying basic features of turbulent flows. The two most frequently studied types of isotropic turbulence are freely decaying, and forced statistically stationary turbulence. For studies in which one wishes stationarity for statistical sampling, forced turbulence is preferable over decaying turbulence. In 2003, a very interesting paper by Lundgren [1] proposed an alternative to the band-limited methods of forcing turbulence, using a linear forcing factor. Apart from its simplicity, the profound advantage of linear forcing is the possibility of applying this method in both physical and Fourier space. Problems that do not admit fully periodic boundary conditions, for instance simulating interactions of turbulence with combustion in which conditions upstream and downstream of the flame are inherently different, are often simulated using numerical codes formulated in physical space, such as finite differences. The application of band-limited forcing schemes requires knowledge of the wavenumbers and Fourier-transformed velocities, quantities that are not readily available in codes formulated in physical space. Rosales and Meneveau[2], in 2005, have shown that the application of linear forcing in both physical and spectral space renders practically equivalent results, reflecting the profound equivalence of the method in both spaces. Thus, the linear-forcing method opens wide opportunities for application in both physical and spectral space. Furthermore, the resemblance of the forcing parameter to an applied shear promises the achievement of stationary spectra, where the structure of the large scale is more realistic. In this direction, Ludgren[1] showed that linear forcing produces statistics at scales between the integral scale and the inertial range (e.g. structure function curving) that resemble the curving observed from experimental data. In 2009, Akylas et al.[3] continued the work of Rosales and Meneveau[2] investigating the statistical stationarity that is produced by applying the linear forcing method in spectral space and quantifying the characteristic scales of the statistically stationary turbulence produced. Furthermore, they presented some arguments on the prediction of the stationary spectra and their importance in initializing linearly forced direct numerical simulations (DNS).

In this work we investigate the linearly forcing method through the Karman-Howarth equation[1,4] in terms of the second and third order structure functions. More specifically, we solve numerically the stationary version using a generalized closure which is based on Oberlack and Peters[5] model, and investigate the behavior of the solutions. We give some theoretical predictions and we present numerical results for the third-order structure function and it is dependence on Reynolds number. The produced forms are in close agreement with experimental data from both homogeneous and non-homogeneous turbulence. Furthermore, we calculate the stationary spectra and we compare them with past DNS of linearly forced turbulence. The model's results are in excellent coincidence and provide a good basis for understanding and initializing linearly forced runs.

STATIONARY ISOTROPIC TURBULENCE BY THE LINEAR FORCING METHOD

Linear forcing is applied in the Navier-Stokes equations by including the linear term $\mathbf{g} = A\mathbf{u}$, proportional to the velocity. The time evolution of the energy spectrum becomes

$$\partial_t E(k,t) = -\partial_k T_k(k,t) - 2\left(\nu k^2 - A\right)E(k,t) \qquad (1)$$

where $T_k(k,t)$ is the function of the spectral transfer of energy. Integrating (1) and taking the energy balance for the statistically stationary state we see that the dissipation rate, ε, is linked with the turbulent kinetic energy, K, through

$$\varepsilon = 2AK = 3Au_{rms}^2 \qquad (2)$$

where u_{rms} is the RMS of the fluctuating velocity. Rosales and Meneveau[2] showed that, independently of the initial conditions, the application of the linear forcing drives the turbulence in a statistical steady state where the turbulent kinetic energy oscillates around an average value, satisfying equation (2). Furthermore, as expected in a statistical sense, this steady state was invariant between runs with a physical space based finite-difference code and runs using standard pseudospectral methods. The above relation (2) between the dissipation and the turbulent kinetic energy is an immediate physical consequence of the energy balance, where the energy injection rate equals the dissipation rate for stationarity. It also defines the characteristic eddy turnover time scale of the turbulence, during the statistically stationary phase,

$$\tau = \frac{u_{rms}^2}{\varepsilon} = \frac{1}{3A} \qquad (3)$$

which could be visualized as the characteristic time lag between energy injection and its eventual dissipation. In order to clarify this, we present, in figure 1, the evolutions of the energy injection rate and the dissipation rate for 30 turnover times (dimensional time 150 for this case).

The results are from linearly forced DNS of isotropic turbulence with a linear forcing parameter A = 0.0666 and viscosity ν = 0.001041 in a $(2\pi)^3$ computational domain, as explained in [3,6]. The two different curves almost coincide when the evolution of the dissipation is shifted forward by the time increment given from equation (3), $t = (3A)^{-1}$.

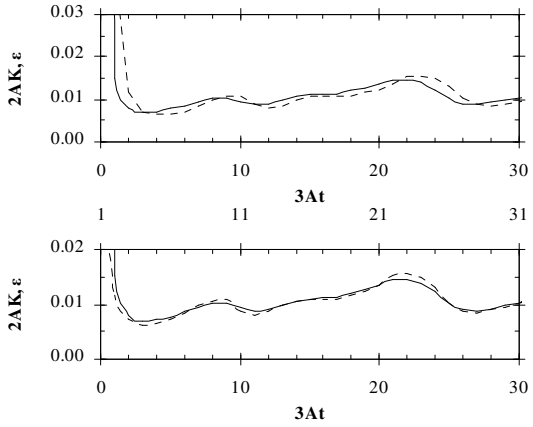

Figure 1. Evolution of the energy injection, $2AK$ (solid line), and dissipation, ε, (dashed line) rates (up). When the dissipation evolution is shifted by $\tau = (3A)^{-1}$, the two curves almost coincide (down).

The same picture can be drawn from the more strict investigation of the correlation between the two evolutions versus their time lag, shown in figure 2. It turns out that the correlation coefficient maximizes when the time difference equals one turnover time-scale. It also implies that in order to retrieve stationary information one needs to average over several turnover times.

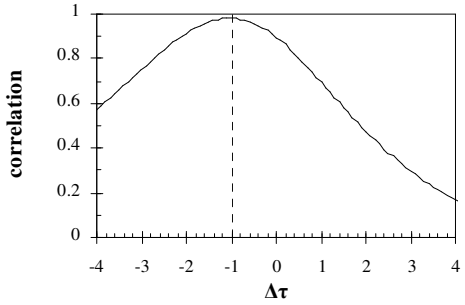

Figure 2. Correlation between the energy injection rate and dissipation rates versus their time difference, for the case presented in figure 1.

What it is not immediately evident is a second, very interesting, relation that links the values of ε and K or u_{rms}, averaged at the stationary phase, with the dimensions of the problem. More specifically, Rosales and Meneveau[2] showed that the energy containing length scale, $L = (2K)^{3/2}/\varepsilon$, characterizing the large eddies, approaches a stationary value, proportional to the dimensions of the problem, l,

$$L = \left(2K\right)^{3/2}/\varepsilon = c \cdot l \approx l \qquad (4)$$

Rosales and Meneveau[2] and Akylas et al.[3] used numerical results from several DNS runs, at different Reynolds numbers

($15<\mathrm{Re}_\lambda<200$), and estimated the constant of the proportionality to be about 1. The constancy of this well-defined stationary length scale L, is supported by the dimensional analysis of the linear forcing method. Apart from the physical interpretation of the linear forcing method, the accurate calculation of c is important because, in combination with equation (2), it defines uniquely the statistics of the application of the linear forcing during the stationary phase[3]. For instance, the turbulent kinetic energy approaches $2K=A^2l^2$, and the averaged dissipation rate, $\varepsilon = A^3l^2$. Also, the values of the Reynolds numbers characterizing the produced stationary isotropic turbulence are uniquely defined using equations (2) and (4).

CHARACTERISTIC SCALES AND SIMILARITY OF LINEARLY FORCED TURBULENCE

The application of the linear forcing in isotropic turbulence imposes a profound time scale which is the reciprocal of the linear forcing parameter A (time^{-1}). The other scales that characterize the application of the linear forcing are the dimension of the box, l (length), and the viscosity, ν (length^2 time^{-1}). The only dimensionless parameter that can be formed combining these scales is then

$$\mathrm{Re}_A = \frac{Al^2}{\nu} \tag{5}$$

which corresponds to a kind of a Reynolds number of the linear forcing and defines the similarity of the problem. Therefore, cases referring to the same value of this parameter should show a similar behavior, approaching the same values of the dimensionless Reynolds number $\mathrm{Re}_L = (2K)^{1/2}L/\nu$, and consequently of $\mathrm{Re}_\lambda = u_{rms}\lambda/\nu$ as well. Using the definition of L and the stationarity implication (2), we express

$$\mathrm{Re}_L = \frac{AL^2}{\nu} \tag{6}$$

and thus, taking the ratio $\mathrm{Re}_L/\mathrm{Re}_A$, we obtain

$$\frac{\mathrm{Re}_L}{\mathrm{Re}_A} = \left(\frac{L}{l}\right)^2 \tag{7}$$

which implies that L should depend only on the box-size, through equation (4). At the same time, using the definition of the Taylor length scale $\lambda_g = (10\nu K/\varepsilon)^{1/2}$, and taking the statistical balance of dissipation and energy injection from equation (2), we see that the Taylor length scale is independent of the box-size, l, depending only on the ratio ν/A, through

$$\lambda_g = 5^{1/2}\lambda = \left(5\frac{\nu}{A}\right)^{1/2} \tag{8}$$

In contrast to the stationary value of L, which depends only on the dimensions of the box (equation 4), the stationary value of λ increases inversely to $(A/\nu)^{1/2}$ through equation (8). The physical interpretation of the Taylor λ scale has the sense of an intermediate scale between the clearly defined and well-separated $\eta = (\nu^3/\varepsilon)^{1/4}$ and L scales (see also Pope[7]). Furthermore, setting $2\nu k_c^2 E(k_c) = 2AE(k_c)$ in equation (1), we determine the specific wave number k_c, where the stationary time-averaged energy production rate equals the stationary time average of the dissipation rate and relates to λ through $k_c = (A/\nu)^{1/2} = \lambda^{-1}$. For this specific value of the wave number, the time-averaged transfer rate $\langle \partial T_k(k_c)/\partial k \rangle$ becomes zero, and the averaged energy transfer function $\langle T_k(k_c) \rangle$ maximizes. As expected from equations (5) – (7), for a given box size (which uniquely defines the length scale $L=l$, through equation 4), the value of the turbulence Reynolds number is proportional to the ratio of the linear forcing divided by the viscosity, A/ν, and hence this ratio defines the dynamical similarity of all linearly forced simulations.

MODELLING THE STRUCTURE FUNCTIONS OF LINEARLY FORCED TURBULENCE

Following the steps presented in [8] the Karman Howarth equation for linearly forced turbulence under statistical stationarity reads [1]

$$-\frac{2}{3}\varepsilon + AB_2 = \frac{1}{6}r^{-4}\partial_r r^4 B_3 - \nu r^{-4}\partial_r r^4 \partial_r B_2 \tag{9}$$

where where B_2 and B_3 are the second- and third-order longitudinal structure functions defined respectively by $B_2(r) = \left\langle [\hat{l}\cdot \mathrm{v}(\mathrm{x}_1 + r\hat{l}) - \hat{l}\cdot \mathrm{v}(\mathrm{x}_1 + r\hat{l})]^2 \right\rangle$, and $B_3(r) = \left\langle [\hat{l}\cdot \mathrm{v}(\mathrm{x}_1 + r\hat{l}) - \hat{l}\cdot \mathrm{v}(\mathrm{x}_1 + r\hat{l})]^3 \right\rangle$, r being the separation between two points in isotropic turbulent flow along the direction defined by $\hat{l}$ .Using the stationarity condition, $\varepsilon = 2AK$, and setting $b_2 = 3B_2/4K$ (so the longitudinal autocorrelation velocity function $f(r) = F(r)/U^2 = 1 - b_2(r)$) equation (9) becomes

$$-1 + b_2 = r^{-4}\frac{\partial_r r^4 B_3}{8AK} - \lambda^2 r^{-4}\partial_r r^4 \partial_r b_2 \tag{10}$$

where, the Taylor λ -scale is given by $\lambda = (\nu/A)^{1/2}$ (note that $\lambda_g = 5^{1/2}\lambda$ and $\lambda_f = 10^{1/2}\lambda$). Furthermore, introducing the dimensionless parameter, $x = r/\lambda$, the Karman_Howarth equation (10) is written

$$-1 + b_2 = x^{-4}\frac{\partial_x x^4 B_3}{8AK\lambda} - x^{-4}\partial_x x^4 \partial_x b_2 \tag{11}$$

We will use the Oberlack and Peters[5] (from here and for the rest OP) model for B_3, and we generalize it, in order to solve (11) and derive spectral information for the steady-state of linearly forced turbulence. The OP model links B_3 to B_2 through

$$B_3(r) = -\frac{6}{5}C_2^{-3/2} r\sqrt{B_2(r)}\partial_r B_2(r)\,. \tag{12}$$

This is the simplest derivative model which relates the Kolmogorov's[9] K41 laws for the second and third order structure functions in the inertial range: for $B_2(r) = C_2(\varepsilon r)^{2/3}$ the third order function becomes $B_3(r) = -4\varepsilon r/5$. Substituting the model equation (12) in the Karman-Howarth equation (9) we get an ordinary differential equation for $B_2(r)$. It is then straightforward to show that for small values of *r* this equation provides the well known result $B_2(r) = \varepsilon r^2/(15\nu) + O(r^4)$. By equation (12) we get $B_3(r) = -(12/5)C_2^{-3/2}(\varepsilon/15\nu)^{3/2} r^3 + O(r^5)$. The velocity derivative skewness, which can be calculated by the formula $S = \lim_{r\to 0} B_3(r)/B_2(r)^{3/2}$, then reads

$$S = -\frac{12}{5}C_2^{-3/2} . \qquad (13)$$

The OP model (4) can be generalized, using different exponents for $B_2(r)$ and its first derivative in equation (12), as follows

$$B_3(r) = -\frac{4}{5}C_2^{-3/2}\left(\frac{3}{2}\right)^a r^a B_2(r)^{(3/2-a)}\left(\partial_r B_2(r)\right)^a \qquad (14)$$

Clearly the choice of a = 1 results to the OP original model. With this generalization, the K41 scaling in the inertial range still holds, and also the skewenness modifies to

$$S = -\frac{12}{5}3^{(-1+a)}C_2^{-3/2} . \qquad (15)$$

Without any implication at this moment, we note that for $C_2 = 2$, the choice of the parameter a = 0.55 results to a value of S = −0.515. Using the general model (14) into (11) the general equation to be solved becomes

$$b_2 + \frac{\partial_x x^4 \partial_x b_2}{x^4} = 1 - \frac{2x^{-4}L}{15\lambda C_2^{3/2}}\left(\frac{3}{2}\right)^{\frac{2a-1}{2}} \partial_x x^{4+a} b_2^{(3/2-a)}\left(\partial_x b_2\right)^a \quad (16)$$

where the energy containing length-scale $L = (2K)^{3/2}/\varepsilon$ and (using the stationarity requirements of the linear forcing) the ratio $L/\lambda = \sqrt{3/5}\,\mathrm{Re}_\lambda$. Rearranging, the eq. (16) we have

$$b_2 + \frac{4b_2'}{x} + b_2'' + D_a x^a b_2^{\frac{3}{2}-a} b_2'^a \left(\frac{4+a}{x} + \frac{3/2-a}{b_2}b_2' + a\frac{b_2''}{b_2'}\right) = 1 \quad (17)$$

where the parameter $D_a = (2/15)C_2^{-3/2}(3/2)^{a-1/2}(L/\lambda)$. The previous equation can be also written in terms of the autocorrelation function $f(x)$ as

$$f + \frac{4f'}{x} + f'' = D_a \frac{\left(-xf'\right)^a}{(1-f)^{a-3/2}}\left(\frac{4+a}{x} - \frac{3/2-a}{1-f}f' + \frac{af''}{f'}\right) \quad (18)$$

The differential equation (18) governing $f(x)$ was solved using the Runge-Kutta (4,5) formula, as applied through the ODE45 MATLAB solver. Given that the ODE is singular at the starting point ($x = 0$), we perturb the initial value, and use instead the point $x = \varepsilon$, where ε is a small number. To calculate the values of f and f' at the new initial point, we obtain a series solution for $f(x)$ near $x = 0$, employing the initial conditions $f(x=0) = 1$ and $f'(x=0) = 0$; that is $f(x) = 1 - x^2/10 + O(x^4)$. The accuracy of the numerical solution was tested with the analytical solution of (18) for the case $\mathrm{Re}_\lambda = 0$,

$$f(x, \mathrm{Re}_\lambda = 0) = [-3\,x\cos(x) + 3\sin(x)]/x^3 \qquad (19)$$

Even for large values of x , there is excellent agreement between numerical and analytical results and the error does not exceed 0.1% . In an analytical approach, for large values of r, we approximate 1 - $f \approx 1$, in (18) and thus we conclude with

$$f + \frac{4f'}{x} + f'' = -D_a(-xf')^a\left[\frac{4+a}{x} - (\frac{3}{2}-a)f' + \frac{af''}{f'}\right] \quad (20)$$

The last form predicts a diminishing behavior for large values of *x* that approaches a power low of the form

$$f(x) \to B_a x^{-z(a)} , \qquad (21)$$

with $z(a) = (1-a)^{-1}$ and $B^{1-a}(a) = D_a(4-5a)/(1-a)^{1+a}$ for values of a in the range $0 \le a < 4/5$. For values of the parameter $a \ge 4/5$, no power low can be drawn. The above results can be verified accurately from the numerical solution of equation (18) for values of the parameter a up to 0.5 (not shown here). Above this value the accuracy of the asymptotic analysis seems to fail due to persisting oscillations. More specifically, for a = 0.57 there is a clear oscillatory behavior around the power low given by equation (21). For a = 0.6 and a = 0.62 the oscillations increase and for a = 0.63 the model collapses due to the negative values of b_2 and b_2' that appear. This behavior could be related to the non-trivial large scales effects associated with the linear forcing. E.g. under the conditions one usually proves the invariance of the Loitsiansky's integral [10,11] one would get that it grows exponentially with time. This behavior can be related, through the influence of the boundary conditions, to the existence and the properties of the stationary state observed in the DNS[13]. A detailed discussion on this fact will be given in the final version of this work after further investigation.

COMPARISONS WITH EXPERIMENTAL DATA AND DIRECT NUMEICAL SIMULATIONS

As it has been described above, equation (18) was solved numerically with MATLAB in order to calculate the B_2 and B_3 structure functions. In this section we present results for the third order structure function and for the resulting isotropic spectra of turbulence.

In order to test the model's predictions for B_3, we have used three different types of air flows: a round jet (at Reynolds numbers 350 and 695), a grid turbulence (at Reynolds numbers 72 and 144) and in the return channel flow of the ONERA-Modane (at Reynolds number 2260). These experimental data are summarized in Gagne et al. (2004)[12]. The respective present model's results have been calculated for the case of the parameter $a = 1$ which corresponds to the original OP model. The value of C_2 was not kept constant but decreases slowly from 2.6 at the lowest Reynolds case to 2.1 for the highest. As it is shown in figure 3 there is remarkable agreement between the model and the experiments although in the case of the jets the shape near the maxima is different. However the overall comparison is good and highlights the physical mechanism of the linearly forcing, which is more natural than a bounded forcing scheme [1]. Different values of the parameter a may result in an even better picture but this is a subject for future research.

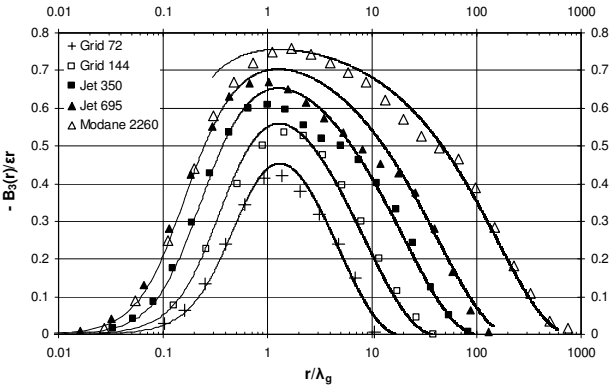

Figure 3. Comparison of the B_3 structure functions calculated by the present model (lines) with experimental data (symbols) from: a round jet at Reynolds numbers 350 and 695, a grid turbulence at Reynolds numbers 72 and 144 and in the return channel flow of the ONERA-Modane.

In order to compare the results of the model against existing DNS data of linearly forced turbulence [2,3], we integrate the calculated autocorrelation function f(r) and calculate the one-dimensional energy spectra as

$$E_{11}(k\lambda)/K\lambda = 4/3\pi\int_0^\infty f(x)\cos(k\lambda x)dx \qquad (22)$$

where $x = r/\lambda$, and K is the turbulent kinetic energy. Furthermore, we differentiate the result of (22) through

$$\frac{E(k\lambda)}{K\lambda} = -\frac{k\lambda}{2}\frac{\partial E_{11}(k\lambda)}{\partial k\lambda} + \frac{(k\lambda)^2}{2}\frac{\partial^2 E_{11}(k\lambda)}{\partial (k\lambda)^2} \qquad (23)$$

and obtain the stationary turbulent kinetic energy spectra of linearly forced turbulence. This step is important, since it may help to predict the forms of the stationary spectra to be used in initializing linearly forced direct numerical simulations. Also it provides with a basis for a more accurate testing of the model's results, against data that refer to the same physical mechanism.

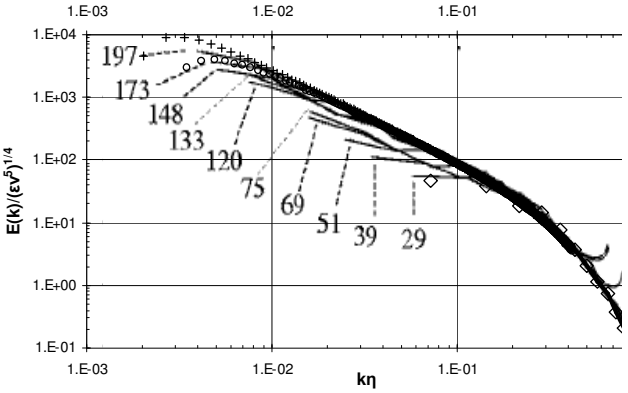

Figure 4. Comparison of the dimensionless turbulent kinetic energy spectra published in [2] (grey lines) with the respective results from the present model (symbols), for Reynolds numbers: 240 (crosses), 173 (circles) and 25 (squares).

On this basis, in figure 4, we compare the dimensionless, turbulent kinetic energy spectra $E(k)/(\varepsilon\nu^5)^{1/4}$, published by Rosales and Meneveau [2] with the respective results from the present model, for a variety of Reynolds numbers. The model results are for values of the parameters $a = 1$ and $C_2 = 2.2$. From the comparison it turns out that the model describes perfectly the stationary spectral forms and performs well within all the wave-number range.

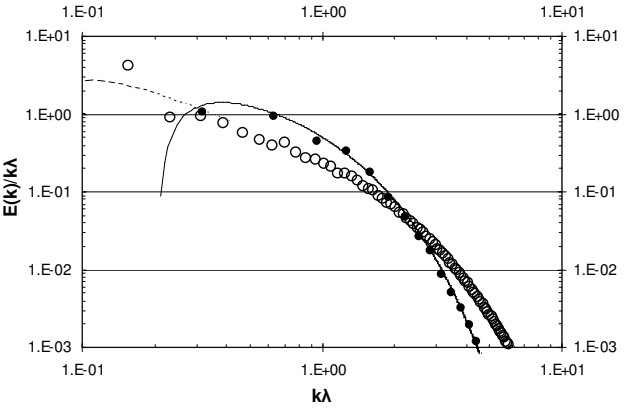

Figure 5. Comparison of the dimensionless turbulent kinetic energy spectra published in [3] (symbols) with the respective results from the present model (lines), for Reynolds numbers: 100 (open circles, spaced-line) and 25 (solid circles, line).

Also, in figure 5, we present the dimensionless, turbulent kinetic energy spectra $E(k)/(k\lambda)$, published by Akylas et al. [3]

and we compare them with the respective results from the present model, for Reynolds number 25 and 100. Once again the model's predictions are in perfect agreement with the DNS. This picture gives the hope that the modeled spectra can be used in initializing linearly forced direct numerical simulations in a future step of this work.

CONCLUSIONS

The physics of the linear forcing of isotropic turbulence, allows for some useful estimates of the characteristic length scales of the turbulence produced during the statistically stationary phase. With such estimates we could practically define uniquely the stationary statistics by means of the box-size of the simulation, the linear forcing parameter and the viscosity of each case. In this work we investigated the linearly forcing method through the Karman-Howarth equation [1,4] in terms of the second and third order structure functions. We solved the stationary version of the equation using a generalized closure which is based on Oberlack and Peters[5] model. The produced forms are in close agreement with experimental data from both homogeneous and non-homogeneous turbulence. Furthermore, the produced stationary spectra of the turbulent kinetic energy are in excellent coincidence with past DNS of linearly forced turbulence. This picture gives the hope that the modeled spectra can be used in initializing linearly forced direct numerical simulations in a future step of this work. The method used still needs further investigation, regarding the role of the exponent (parameter a) in the generalized OP model and the values of the parameter C_2, but it provides a good basis for understanding and possibly initializing linearly forced runs.

Aknowledgment This work was partially supported by PRIMA, a Marie Curie Reintegration Grant. The first author would like to dedicate this work to the memory of Arietta.

REFERENCES

[1] Lundgren T.S. (2003), "Linearly forced isotropic turbulence", in Annual Research Briefs of Center for Turbulence Research, Stanford, pp. 461- 473

[2] Rosales, C., and Meneveau, C. (2005), "Linear forcing in numerical simulations of isotropic turbulence: Physical space implementations and convergence properties", Phys. Fluids, Vol. 17, 095106

[3] Akylas, E., Kassinos, S.C., Rousson, D. and Xu, X. (2009), "Accelerating Stationarity in Linearly Forced Isotropic Turbulence". Proc. of the 6th International Symposium on Turbulence and Shear Flow Phenomena, Seoul Korea, 22–24 June 2009.

[4] Von Karman, T. and Howarth, L. (1938), "On the statistical theory of isotropic turbulence", Proc. Roy. Soc. Lond. A 164, 192-215.

[5] Oberlack, M., and Peters, N. (1993), "Closure of the two-point correlation equation in physical space as a basis for Reynolds stress models", *Near Wall Turbulent Flows*, edited by R. M. C. So, C.G. Speziale, and B.E. Launder (Elsevier, Amsterdam, 1993).

[6] Kassinos, S.C, Knaepen, B., and Carati, D. (2007), "The transport of a passive scalar in magnetohydro-dynamic turbulence subjected to mean shear and frame rotation", Phys. Fluids, Vol. 17(1), 015105

[7] Pope S.B. (2000), *Turbulent flows*, Cambridge University Press, 2000, pp. 421

[8] Landau, L. D. and Lifshitz, E. M. (1959), *Fluid Mechanics*, Pergamon, London.

[9] Kolmogorov, A. N. (1941), "The local structure of turbulence in incompressible viscous fluid for very large Reynolds numbers", Dokl. Akad. Nauk., SSSR 30, 299-303. Reprinted in Proc. Roy. Soc. London A 434, 9-13 (1991).

[10] P. G. Saffman, P.G. (1967), ''Note on the decay of homogeneous turbulence'', Phys. Fluids 10, 1349- 1967.

[11] Monin and Yaglom A.M., *Statistical Fluid Mechanics: Mechanics of Turbulence*, MIT Press, Cambridge, MA, Vol. 2.

[12] Gagne, Y., Castaing, B., Baudet, C. and Malecot, Y. (2004), "Reynolds dependence of third-order velocity structure functions", Physics of Fluids, 16, 482–485.

[13] Gravanis E. and E. Akylas, On the stationarity of linearly forced turbulence in finite domains, pre-print arXiv:1104.5323.